Materials Letters 400 (2025) 139186

Contents lists available at ScienceDirect

Materials Letters

journal homepage: www.elsevier.com/locate/matlet

Ultrafine Ru on reduced graphene oxide-La_2O_3 binary support for highly efficient hydrogen evolution reaction

Jiaying Zhang [a], Qijing Zhang [a], Jingyi Qiu [a], Xiaoying Zhang [a], Zhiyuan Zhu [a], Hongyan Chen [a], Konggang Qu [a,*], Lijian Meng [b,*]

[a] School of Chemistry and Chemical Engineering, Shandong Provincial Key Laboratory/Collaborative Innovation Center of Chemical Energy Storage & Novel Cell Technology, Liaocheng University, Liaocheng 252059, China
[b] Centre of Innovation in Engineering and Industrial Technology, Instituto Superior de Engenharia do Porto, Instituto Politecnico do Porto 4249-015 Porto, Portugal

ARTICLE INFO

Keywords:
Ru nanoparticle
Hydrogen evolution reaction
Reduced graphene oxide
La_2O_3
Electrocatalyst

ABSTRACT

Ru-based catalysts are recognized as one of the most competitive candidates for hydrogen evolution reaction (HER). Nonetheless, reducing Ru loading and maximizing atomic utilization remain paramount priorities for achieving optimal cost efficiency. Herein, the ultrafine Ru nanoparticles loaded on a reduced graphene oxide-La_2O_3 binary support (Ru/La_2O_3-rGO) was rationally designed via a simple liquid impregnation method with a low-content Ru of 6.1 wt%. Benefitting from the synergistic interplay of the binary substrate, Ru/La_2O_3-rGO achieves a current density of 10 mA cm^{-2} at an ultrasmall overpotential of 15.8 mV for alkaline HER, outperforming Pt/C, while also exhibiting good stability and high intrinsic activity. This work offers novel insights into the rational design of high-performance, stable, and cost-effective Ru-based HER catalysts.

1. Introduction

Platinum (Pt) is the benchmark electrocatalyst for the cathodic hydrogen evolution reaction (HER) in water splitting [1]. Unfortunately, the high cost and scarcity of Pt severely hinder its widespread adoption. Ru-based catalysts are now recognized as the most competitive alternatives, offering Pt-like activity, superior chemical stability and significantly lower cost [2]. However, as Ru remains a noble metal, reducing its loading and maximizing atomic utilization are still critical for achieving optimal cost efficiency. Recently, rare-earth elements and their oxides have demonstrated remarkable advantages as supports for heterogeneous catalysts. In particular, La_2O_3 possesses a unique electronic structure and promoter effects for metal catalysts due to the abundant electronic energy levels in La and strong metal-support interactions [3,4]. However, the inherent non-conductivity of La_2O_3 limits its electrocatalytic performance and must be addressed. Reduced graphene oxide (rGO) is recognized as an ideal support due to its unique two-dimensional structure, high conductivity, and large specific surface area [5].

In this work, we propose the design of ultrafine Ru loaded on a La_2O_3-rGO binary support with a low content of Ru (6.1 wt%). The resulting catalyst achieves 10 mA cm^{-2} at an ultrasmall overpotential of 15.8 mV, with a Tafel slope of 48.59 mV dec^{-1} and excellent stability for alkaline HER, surpassing Pt/C.

2. Experimental procedure

2.1. Synthesis of La_2O_3-GO composite

GO was obtained according to our previous procedure [6]. 50 mg of GO was dispersed in 50 mL of ultrapure water and ultrasonicated for 30 min to form a reddish-brown suspension. The pH was adjusted to 10.5 using aqueous ammonia. Subsequently, a solution containing 50 mg of $La(NO_3)_3{\cdot}6H_2O$ in 5 mL of water was added dropwise into the mixture, followed by 30 min of stirring. Then, a solution of 40 mg NaOH in 5 mL of water was added. After overnight stirring, the precipitate was collected by centrifugation, washed repeatedly to neutral pH, and dried at 80 °C to obtain La_2O_3-GO composite.

2.2. Synthesis of La_2O_3-rGO

La_2O_3-rGO was synthesized by directly pyrolyzing La_2O_3-GO at 600 °C under a mixed H_2/Ar atmosphere (volume ratio 5:95) for 2 h.

* Corresponding authors.
E-mail addresses: qukonggang@lcu.edu.cn (K. Qu), ljm@isep.ipp.pt (L. Meng).

https://doi.org/10.1016/j.matlet.2025.139186
Received 19 May 2025; Received in revised form 21 July 2025; Accepted 27 July 2025
Available online 28 July 2025

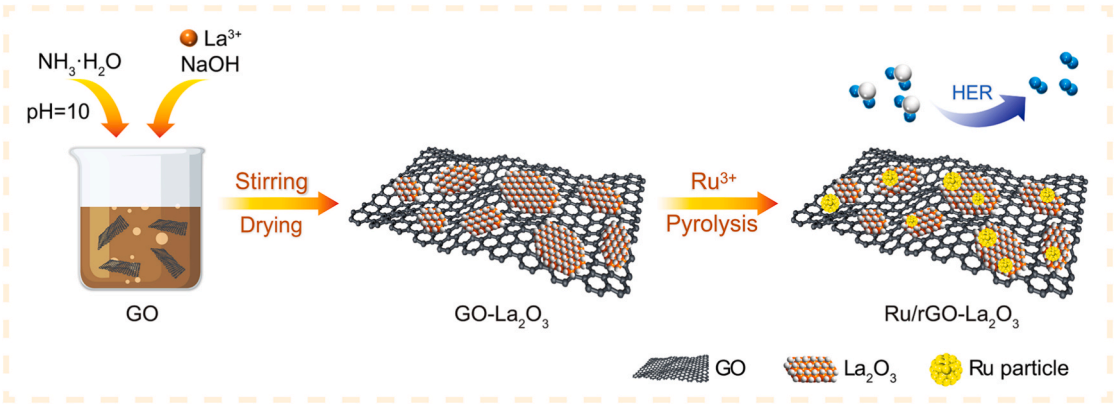

Fig. 1. Synthesis route of Ru/La_2O_3-rGO.

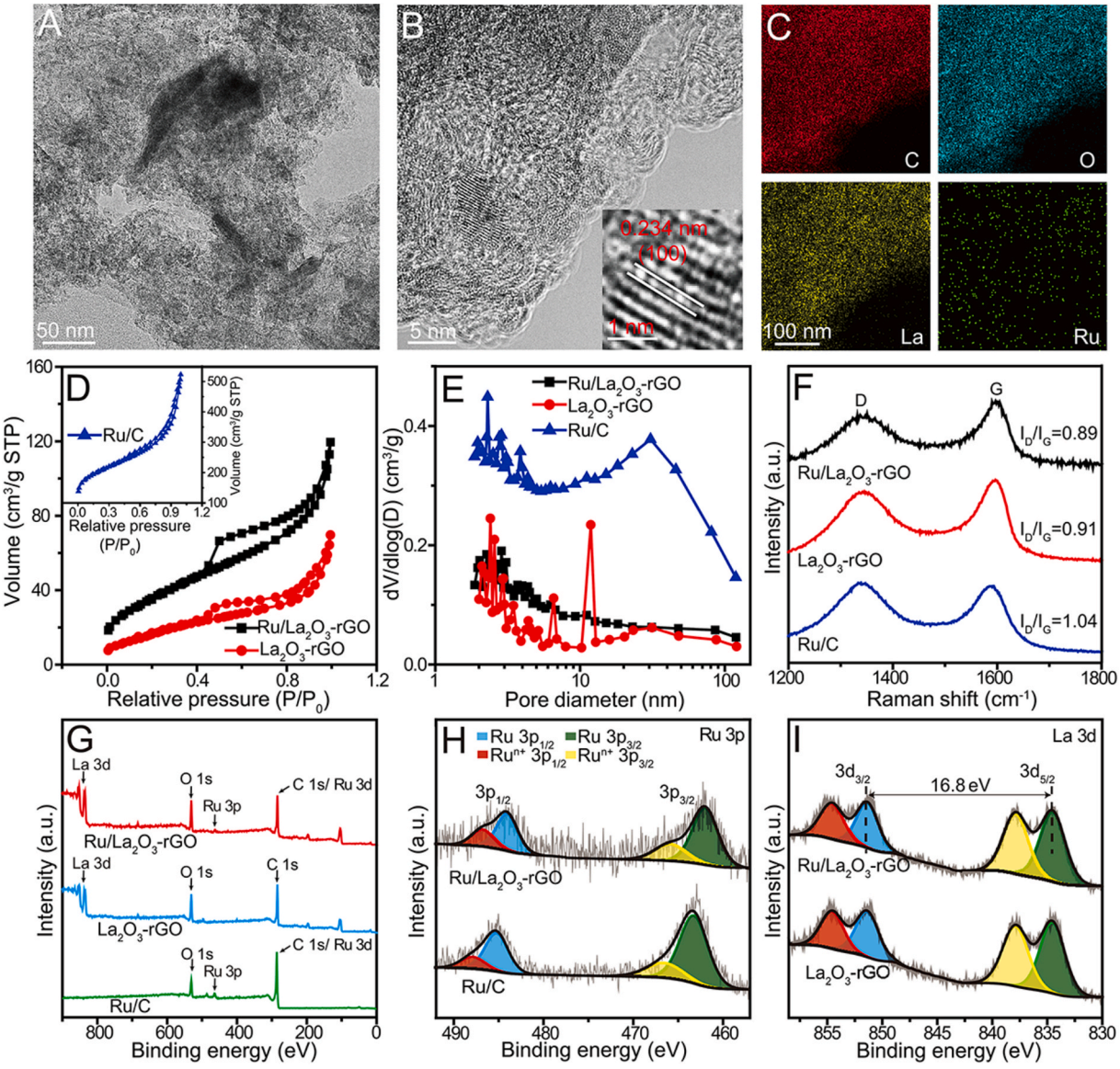

Fig. 2. (A-B) TEM images at different magnifications and (C) TEM elemental mapping of Ru/La_2O_3-rGO. (D) N_2 isotherm curves and (E) the pore size distribution curves. (F) Raman spectra. (G) XPS survey scan and high-resolution XPS spectra of (H) Ru 3p and (I) La 3d.

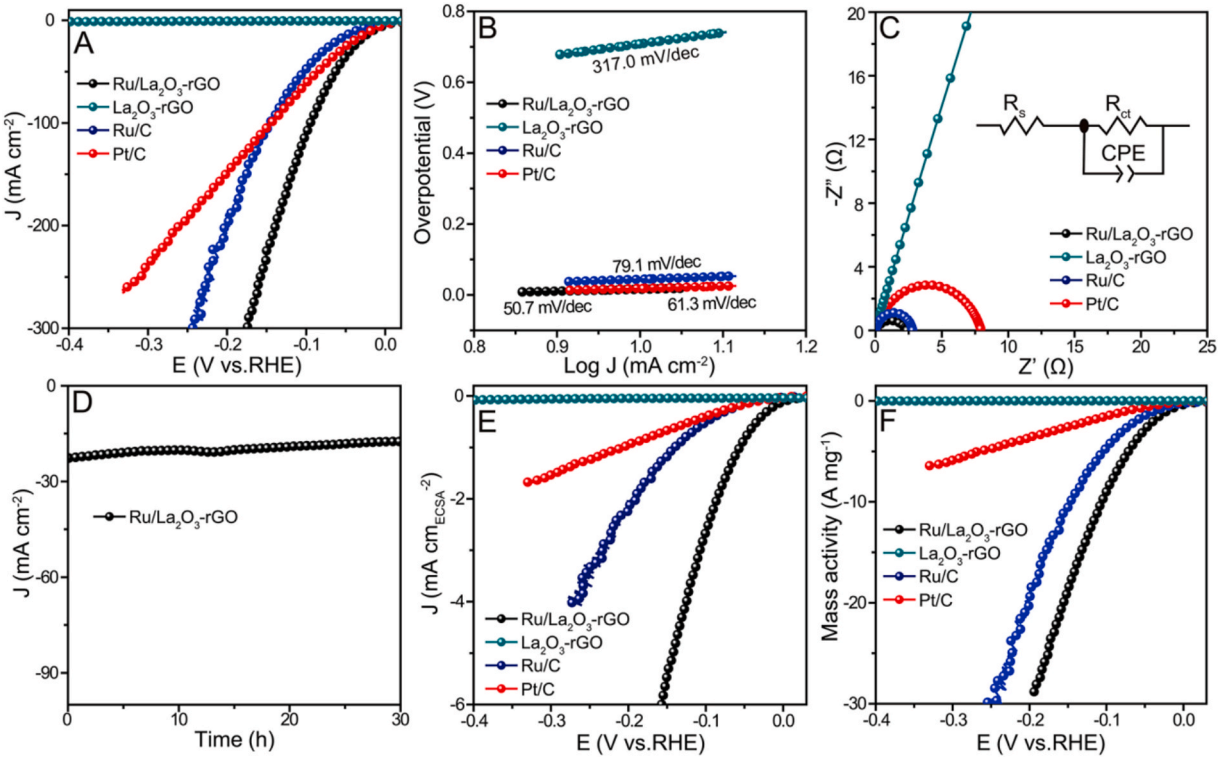

Fig. 3. (A) HER LSV curve of Ru/La_2O_3-rGO, La_2O_3-rGO and Ru/C in 1.0 M KOH solution. (B) Tafel Slope of catalysts. (C) EIS of catalysts. (D) The chronoamperometric curve of Ru/La_2O_3-rGO. (E) ECSA normalized LSV curve of catalysts. (F) Mass activity curve of catalysts.

2.3. Synthesis of Ru/La$_2$O$_3$-rGO

20 mg of La_2O_3-GO was dispersed in 10 mL ultrapure water, followed by the addition of 2.16 mg $RuCl_3{\cdot}xH_2O$ and stirring for 4 h. The precipitate was collected by centrifugation, dried at 80 °C, and then pyrolyzed at 600 °C under a mixed H_2/Ar atmosphere (volume ratio 5:95) for 2 h. The resulting sample was named as Ru/La_2O_3-rGO.

3. Results and discussion

The novel Ru/La_2O_3-rGO catalyst was synthesized as illustrated in Fig. 1. The morphological features of the samples were characterized by transmission electron microscopy (TEM). As shown in Fig. 2A, Ru/La_2O_3–rGO exhibits a layered structure, with amorphous La_2O_3 domains and ultrafine Ru particles (~4 nm). The lattice fringes of 0.234 nm correspond to the Ru (1 0 0) plane of the hexagonal close-packed (hcp) crystal phase (Fig. 2B) [7]. Elemental mapping images (Fig. 2C) confirm the coexistence of C, O, La, and Ru. TEM images of La_2O_3-rGO (Fig. S1) reveal a similar layered structure and amorphous La_2O_3. The inductively coupled plasma optical emission spectroscopy (ICP-OES) analysis verifies the contents of 6.1 wt% Ru and 44.9 wt% La, indicating Ru/La_2O_3-rGO contains approximately 6.1 wt% Ru, 52.7 wt% La_2O_3, and 41.2 wt% rGO. These results suggest that the La_2O_3-rGO composite serves as an ideal platform for anchoring and dispersing Ru nanoparticles.

Fig. 2D depicts the N_2 adsorption–desorption isotherms. The Brunauer-Emmett-Teller (BET) surface area of Ru/La_2O_3-rGO is 132.7 $m^2\ g^{-1}$, with an average pore diameter of 5.85 nm (Fig. 2E and Table S1), compared to La_2O_3-rGO (65.5 $m^2\ g^{-1}$ and 6.25 nm) and commercial Ru/C (664.2 $m^2\ g^{-1}$ and 7.58 nm) [8]. The carbon structure was assessed by Raman spectroscopy. Fig. 2F reveals the D and G bands observed at 1350 cm^{-1} and 1596 cm^{-1}, respectively. Ru/La_2O_3-rGO exhibits the lowest intensity ratio of D band and G band (I_D/I_G, 0.89), compared to La_2O_3-rGO (0.91) and Ru/C (1.04), indicating the highest degree of graphitization and thus favorable electronic conductivity during electrocatalysis.

The surface chemical states were analyzed by X-ray photoelectron spectroscopy (XPS). Fig. 2G displays the full spectra of different samples, confirming the presence of C, O, La, and Ru in Ru/La_2O_3-rGO. As shown in Fig. 2H, Ru 3p spectra contain two pairs of peaks. The peaks at 462.0 and 484.0 eV corresponds to the $3p_{3/2}$ and $3p_{1/2}$ of Ru^0, with those at 465.9 and 486.8 eV are attributed to Ru^{n+} species [2]. Notably, both the Ru^0 3p and 3d peaks in Ru/La_2O_3-rGO exhibit a shift of approximately 1.28 eV toward lower binding energy compared to Ru/C, indicating increased electron density around Ru [9,10]. The La 3d high-resolution spectra of Ru/La_2O_3-rGO (Fig. 2I) show four peaks at 834.5 and 837.9 eV (La $3d_{5/2}$), and 851.3 and 854.6 eV (La $3d_{3/2}$). The spin–orbit energy splitting between La $3d_{3/2}$ and La $3d_{5/2}$ peaks is 16.8 eV, a typical feature of La_2O_3 species [11,12].

The HER activity was evaluated in a three-electrode electrolytic cell. Linear sweep voltammetry (LSV) curves in 1.0 M KOH are shown in Fig. 3A [6]. Ru/La_2O_3-rGO requires only a minimal overpotential of 15.8 mV to reach a current density of 10 mA cm^{-2}, outperforming Pt/C (18.4 mV) and Ru/C (36.7 mV), and is comparable to recently reported materials (Table S2). Remarkably, Ru/La_2O_3-rGO exhibits exceptional performance at high current density, attaining 100 mA cm^{-2} at a significantly lower overpotential of 94.3 mV, surpassing Pt/C (143.9 mV) and Ru/C (145.7 mV). Tafel slopes, a key metric for evaluating HER kinetics, are presented in Fig. 3B [1]. Ru/La_2O_3-rGO exhibits the lowest Tafel slope of 50.7 mV dec^{-1}, indicating accelerated HER kinetics, superior to Pt/C (61.3 mV dec^{-1}) and Ru/C (79.1 mV dec^{-1}). Electrochemical impedance spectroscopy (EIS) further reveals a charge transfer resistance (R_{ct}) of 2.37 Ω for Ru/La_2O_3-rGO (Fig. 3C), lower than that of Pt/C (7.93 Ω) and Ru/C (2.80 Ω), confirming that the La_2O_3-rGO support facilitates electron transfer during electrolysis. Stability, a critical factor for practical applications, was assessed via chronoamperometry (Fig. 3D) [7]. Ru/La_2O_3-rGO maintains a nearly constant current density over 30 h, demonstrating exceptional operational durability, likely due to strong interfacial interactions between Ru and La_2O_3-rGO support. XPS characterization after stability test (Fig. S2) indicates the Ru component in Ru/La_2O_3-rGO remains nearly unchanged. However, the

La 3d spectra are more consistent with those of $La(OH)_3$, as evidenced by a bind energy difference of 3.5 eV between two La $3d_{5/2}$ peaks [13]. This suggests that La_2O_3 is readily converted to $La(OH)_3$, which is reasonable given the basic environment.

To evaluate the intrinsic activity of the samples, the electrochemical surface area (ECSA)-normalized and mass-activity LSVs was analyzed (Fig. S3, 3E and F) [14]. Specifically, Ru/La_2O_3-rGO achieves −2.65 mA cm^{-2}_{ECSA} at −0.1 V, which is 6.6 and 5.1 times higher than Pt/C (−0.40 mA cm^{-2}_{ECSA}) and Ru/C (−0.52 mA cm^{-2}_{ECSA}), respectively, highlighting the superior intrinsic activity of Ru/La_2O_3-rGO [12].The mass activity of −9.01 A mg^{-1} at −0.1 V is 5.9 and 1.9 times higher than that of Pt/C (−1.52 A mg^{-1}) and Ru/C (−4.71 A mg^{-1}), respectively, demonstrating the superior atomic utilization efficiency of Ru/La_2O_3-rGO [14].

4. Conclusions

In conclusion, a simple and efficient liquid impregnation strategy was employed to synthesize Ru/La_2O_3-rGO. The binary support, integrating rGO and La_2O_3, synergistically enables uniform dispersion, modulates the electronic structure of Ru, and ensures favorable electrical conductivity. As a result, Ru/La_2O_3-rGO with a low Ru content of 6.1 wt% achieves a current density of 10 mA cm^{-2} at an overpotential of only 15.8 mV for alkaline HER, with excellent stability and high intrinsic activity, surpassing commercial Pt/C. This study opens a new avenue for designing cost-effective, highly active, and durable Ru-based catalysts.

CRediT authorship contribution statement

Jiaying Zhang: Writing – original draft, Methodology, Conceptualization. **Qijing Zhang:** Formal analysis, Conceptualization. **Jingyi Qiu:** Validation, Investigation. **Xiaoying Zhang:** Writing – original draft, Methodology, Conceptualization. **Zhiyuan Zhu:** Validation, Investigation. **Hongyan Chen:** Resources, Project administration. **Konggang Qu:** Writing – review & editing, Supervision, Funding acquisition. **Lijian Meng:** Writing – review & editing, Supervision.

Declaration of competing interest

The authors declare that they have no known competing financial interests or personal relationships that could have appeared to influence the work reported in this paper.

Acknowledgements

This work was financially supported by the Development Project of Youth Innovation Team in Shandong Colleges and Universities (2019KJC031), Natural Science Foundation of Shandong Province (ZR2022MB137) and Doctoral Program of Liaocheng University (318051608).

Appendix A. Supplementary data

Supplementary data to this article can be found online at https://doi.org/10.1016/j.matlet.2025.139186.

Data availability

Data will be made available on request.

References

[1] F.-W. Chen, S.-N. Zhang, J.-J. Li, A.M. Kan, M. Yang, J. Zhao, G. Deng, Mater. Lett. 309 (2022) 131470.
[2] K.-G. Qu, Z.-F. Chen, L.-H. Wang, H.-B. Li, S.-Y. Zeng, R. Li, L.-J. Meng, H.-Y. Chen, Q.-X. Yao, Rare Met. 44 (2025) 2094–2102.
[3] T. Xia, J. Wang, N. Lin, L. Huo, H. Zhao, G. Mountrichas, J. Alloys Compd. 507 (2010) 245–252.
[4] Z. Barandiarán, L. Seijo, J. Chem. Phys. 119 (2003) 3785–3790.
[5] Y. Feng, S. Zhang, L. Zhu, G. Li, N. Zhao, H. Zhang, B.H. Chen, Int. J. Hydrogen Energy 47 (2022) 39853–39863.
[6] K. Qu, Y. Zheng, X. Zhang, K. Davey, S. Dai, S.Z. Qiao, ACS Nano 11 (2017) 7293–7300.
[7] X. Guan, Q. Wu, H. Li, S. Zeng, Q. Yao, R. Li, H. Chen, Y. Zheng, K. Qu, Appl. Catal. B Environ. 323 (2023) 122145.
[8] X. Zhang, L. Liu, J. Wang, X. Ju, R. Si, J. Feng, J. Guo, P. Chen, J. Catal. 417 (2023) 382–395.
[9] H. Sun, Z. Yan, C. Tian, C. Li, X. Feng, R. Huang, Y. Lan, J. Chen, C.-P. Li, Z. Zhang, M. Du, Nat. Commun. 13 (2022) 3857.
[10] L. Chong, G. Gao, J. Wen, H. Li, H. Xu, Z. Green, J.D. Sugar, A.J. Kropf, W. Xu, X.-M. Lin, H. Xu, L.-W. Wang, D.-J. Liu, Science 380 (2023) 609–616.
[11] T. Honma, Y. Benino, T. Fujiwara, T. Komatsu, R. Sato, V. Dimitrov, J. Appl. Phys. 91 (2002) 2942–2950.
[12] Y. Li, B. Guan, A. Maclennan, Y. Hu, D. Li, J. Zhao, Y. Wang, H. Zhang, Electrochim. Acta 241 (2017) 395–405.
[13] L.P. Lingamdinne, J.-S. Choi, Y.-L. Choi, Y.-Y. Chang, J.R. Koduru, Chemosphere 313 (2023) 137615.
[14] X. Guan, Y. Sun, S. Zhao, H. Li, S. Zeng, Q. Yao, R. Li, H. Chen, K. Qu, SusMat 4 (2024) 166–177.